AIAA JOURNAL
Vol. 31, No. 9, September 1993

Model for Entropy Production and Pressure Variation in Confined Turbulent Mixing

Dimitri Papamoschou*
University of California, Irvine, Irvine, California 92717

A quasi-one-dimensional model for the planar, confined shear layer is constructed with the purpose of obtaining estimates of entropy production and pressure variation due to turbulent mixing. The turbulent Prandtl and Lewis numbers are assumed to be unity. It is found that entropy production is strongly coupled to the intrinsic compressibility, with total pressure losses becoming significant as the convective Mach number increases. For the isothermal case, the entropy flux is roughly proportional to the third power of the velocity difference, and the equivalent total pressure ratio decays exponentially with the square of the convective Mach number. Pressure gradients in a parallel channel are strong and adverse at high compressibility levels. The model predictions of equivalent total pressure ratio and shear-layer displacement thickness compare well with existing experimental data.

Nomenclature

a = speed of sound
C = mass fraction
c_p = specific heat at constant pressure
c_v = specific heat at constant volume
H = total enthalpy
h = static enthalpy
M = Mach number
M_c = convective Mach number
$\dot{m}$ = mass flux
p = pressure
q = heat transfer
R = gas constant
$\dot{S}$ = entropy flux
s = entropy
T = temperature
U = velocity
x = streamwise coordinate
Y = stream height (area)
y = transverse coordinate
α = channel divergence angle
γ = specific-heat ratio
ΔU = $U_{\infty 1} - U_{\infty 2}$
ΔT = $T_{\infty 1} - T_{\infty 2}$
δ = shear-layer thickness
μ = viscosity
ρ = density
τ = shear stress
ψ = equivalent total pressure ratio, Eq. (35)
ω = mass transfer

Subscripts

avg = average of freestream values
dsl = dividing streamline
T = total (stagnation)
W = wall
zpg = zero pressure gradient
0 = initial conditions ($x = 0$)
1 = stream 1 (fast)
2 = stream 2 (slow)
12 = combined streams 1 and 2
∞ = freestream conditions

Received May 21, 1992; revision received Oct. 24, 1992; accepted for publication Oct. 28, 1992.

*Assistant Professor, Department of Aerospace and Mechanical Engineering. Member AIAA.

Introduction

HIGH-SPEED mixing is a rapidly developing area of fluid mechanics, motivated primarily by the advent of supersonic-combustion ramjet (scramjet) engines. From the practical point of view, two issues are central to the efficient operation of scramjets: good fuel-to-air mixing and minimization of total pressure losses. The fact that air flow inside the combustion chamber is supersonic makes both goals extremely challenging. Although there is a multitude of ways one can inject gaseous fuel into air, they can broadly be classified into two: transverse injection and parallel injection. Transverse injection may produce good near-field mixing but is inevitably accompanied by shocks which reduce the total pressure. Parallel injection, on the other hand, could conceivably be achieved without shocks but may require long combustor lengths for adequate mixing. The question then is, what are the fluid-mechanical losses inherent to mixing of parallel heterogeneous streams in a channel long enough to allow the desired level of mixing? This is the main point this report tries to address.

Several issues related to two-stream, confined mixing were initially explored by Ferri and Edelman[1] and by Ferri.[2] In particular, conditions were derived for multiple-stream choking and for the sign of pressure variation between initial and uniformly mixed conditions. The difficulties of predicting the flow behavior were underscored. More recently, Dutton et al.[3] studied the pressure recovery in a constant area, supersonic-supersonic ejector. It was found that the pressure rise between unmixed and nearly uniformly mixed conditions is similar to that associated with a normal shock in a single-stream equivalent flow. The flow deceleration to subsonic speeds is the combined result of wall shear, mixing, shocks, and boundary-layer separation. This type of ejector performance, which occurs when the two fluids are completely mixed, is clearly undesirable for a scramjet. Therefore, we will examine mixing up to the point where the mixing region occupies some fraction of, but not the entire, channel. The two-dimensional, shear-layer configuration will be considered. The analysis will focus on the generation of entropy due to mixing alone, without any shock waves, and on axial pressure variation.

What enables today a more informed look at the high-speed, confined mixing problem—compared to, say, 10 years ago—is the rapidly growing knowledge of supersonic shear layers and of compressible turbulence in general. The centerpiece of the analysis that follows is the Reynolds shear stress and its dependence on flow parameters. There is now enough

experimental information to construct an approximate model for that dependence. Although the supersonic shear-layer experiments in the literature have not addressed the issue of entropy rise and have not studied systematically the pressure variation, they provide valuable data which are used as empirical inputs to the model.

Quasi-One-Dimensional Description of Shear Layer

There are several instances in compressible flow where two-dimensional problems with friction and/or heat transfer are analyzed as one dimensional, with the shear stress and heating or cooling applied artificially on the fluid. Celebrated examples are the Fanno and Rayleigh flows, widely used for estimating head losses of compressible flow in pipes. Even though the simplification appears drastic, the estimates provided by such methods are quite accurate. Of course, empirical inputs are needed for the models to work. In Fanno flow, for example, such input is the friction factor which is well known vs Reynolds number, Mach number, and pipe roughness. The Fanno and Rayleigh methods can easily be extended to variable-area channels,[4] in which case the analyses become quasi-one-dimensional.

The approach of this study is to treat the planar shear layer as composed of two quasi-one-dimensional streams, confined within a channel with adiabatic walls. The transformation from the two-dimensional to the quasi-one-dimensional description is shown in Fig. 1. In both descriptions, the static pressure is assumed uniform in the crossplane direction, $p = p(x)$. The two streams are separated by the dividing streamline, hence each stream preserves its mass flux $\dot{m}$. The shape of the dividing streamline is initially unknown and is found by the computational scheme described herein.

The smoothly varying velocity profile shown in the two-dimensional description is replaced by two uniform velocities U_1 and U_2. The same occurs with all the other variables. Even though we lose all details of the transverse gradients of velocity, temperature, and composition, we retain the main effects of those gradients, namely, the shear stresses, heat transfer, and mass transfer, which are now artificially applied on the quasi-one-dimensional flowfield. The application of the shear stresses is shown in Fig. 1: for the fast stream, the stresses $-\tau_{dsl}$ on the dividing streamline and $-\tau_{W1}$ on the upper wall; both oppose the fluid motion. For the slow stream, the stress on the dividing streamline $+\tau_{dsl}$ acts toward the flow direction (can be thought of as "negative" friction) whereas a stress $-\tau_{W2}$ acts on the lower wall. In the two-dimensional description, the flow external to the shear layer and boundary layers ("freestream" flow) is assumed isentropic. This is important, because the shear stresses depend on the freestream quantities and not on the averaged, quasi-one-dimensional quantities. Finding the freestream values is easy once the static pressure is known from the quasi-one-dimensional calculation.

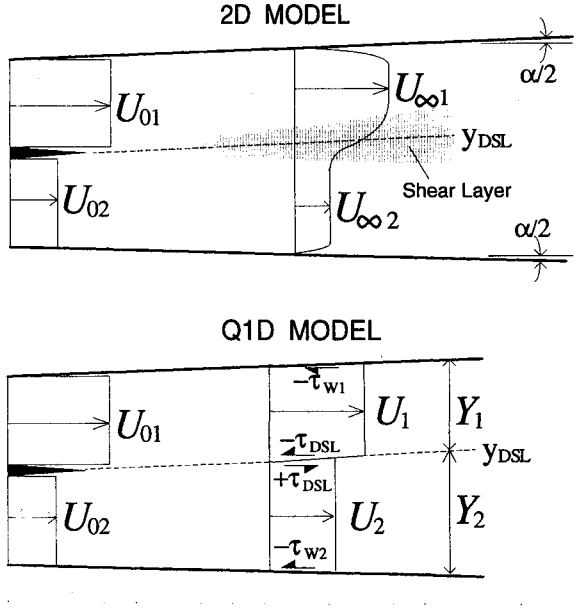

Fig. 1 Two-dimensional (2D) and quasi-one-dimensional (Q1D) descriptions of shear layer.

The validity of the model, therefore, depends on provision of reasonable inputs for the shear stress, heat transfer, and mass transfer. We are particularly interested in the shear layer and not so much in the boundary layers whose properties are well known. For the shear layer, it can be shown that, subject to certain assumptions, the heat and mass transfer are proportional to the shear stress. Hence, it is crucial to establish a relation for τ_{dsl} which would work for variable velocity ratio, density ratio, and Mach number.

Model for the Reynolds Stress

Following an argument similar to Brown and Roshko's,[5] the Eulerian version of the momentum equation gives an estimate for the maximum shear stress

$$\tau_{max} \sim \frac{d\delta}{dx}\rho_{avg}U_{avg}\Delta U \tag{1}$$

where U_{avg} represents the mean velocity at which momentum is transported, here assumed to be the average of the freestream velocities; ΔU is the difference of the freestream velocities; and $d\delta/dx$ is the turbulent shear-layer growth rate. It is also assumed that the density at $\tau = \tau_{max}$ is close to the average density ρ_{avg}.

Recent experiments[6-9] have shown that the turbulent shear-layer growth rate is adequately described by the relation

$$\frac{d\delta}{dx} \sim \frac{\Delta U}{U_c} f(M_c) \tag{2}$$

where U_c is the "convective velocity" of the large-scale structures given by

$$U_c = \frac{U_{\infty 1} + U_{\infty 2}\sqrt{\rho_{\infty 2}/\rho_{\infty 1}}}{1 + \sqrt{\rho_{\infty 2}/\rho_{\infty 1}}} \tag{3}$$

M_c is the convective Mach number

$$M_c = \frac{\Delta U}{a_{\infty 1} + a_{\infty 2}} \tag{4}$$

and $f(M_c)$ is a compressibility function such that $f(0) = 1$. Specializing Eq. (2) to the pitot thickness (close to visual thickness), we can write it as an equality

$$\frac{d\delta}{dx} = 0.17\frac{\Delta U}{U_c} f(M_c) \tag{5}$$

the constant of 0.17 having been obtained experimentally.[6]

Combining Eqs. (1) and (2) we obtain the following estimate for the shear stress:

$$\tau_{max} = c_\tau \rho_{avg}(\Delta U)^2 \frac{U_{avg}}{U_c} f(M_c) \tag{6}$$

where c_τ is a constant obtained from subsonic, equal-density experiments. Here we use Wygnanski and Fiedler's[10] value $c_\tau = 0.013$.

The compressibility function $f(M_c)$ can be extracted from growth-rate data[6-9] or direct laser-Doppler velocimeter (LDV) measurements of the quantity $-\overline{u'v'}$ performed in supersonic shear layers.[7,11] Note that, for compressible flow, the Reynolds stress is

$$\tau = -\bar{\rho}\overline{u'v'} - \bar{u}\overline{\rho'v'} - \bar{v}\overline{\rho'u'} - \overline{\rho'u'v'}$$

At high Mach number, the density-velocity double correlations could become significant, so measurement of $-\overline{u'v'}$ alone may not accurately represent the shear stress. Of course, measurement of density-velocity correlations is at present extremely difficult.

In this report, both growth-rate and $\overline{u'v'}$ data are used to infer the compressibility function $f(M_c)$. A compilation of data from several investigations is shown in Fig. 2. The $\overline{u'v'}$ measurements seem to underpredict the stabilizing effect of compressibility, which could be attributed to the observation in the previous paragraph. An approximate curve fit, which gives roughly equal weight to the $\overline{u'v'}$ data and to the growth-rate data, provides the estimate

$$f(M_c) \approx 0.25 + 0.75e^{-3M_c^2} \tag{7}$$

The scatter of the experimental data seen in Fig. 2 will introduce an uncertainty of roughly 20% in the predictions of entropy generation and pressure variation. Several trials have shown that the sign of the pressure gradient, i.e., whether static pressure increases or decreases in a constant-area configuration, is largely unaffected by the scatter in $f(M_c)$.

To make the connection between $\tau_{\max}$ and τ_{dsl}, we note that in a self-similar shear layer with zero pressure gradient, the maximum shear stress occurs on the dividing streamline,[12] i.e., $\tau_{dsl} = \tau_{\max}$. It seems reasonable to expect that, in the presence of a modest pressure gradient, the preceding equality will still hold approximately. We now summarize the foregoing arguments and relationships into an expression for τ_{dsl}

$$\tau_{dsl} = 0.013\rho_{avg}(\Delta U)^2\left[\frac{1+\sqrt{\rho_{\infty 2}/\rho_{\infty 1}}}{2} \times \frac{U_{\infty 1}+U_{\infty 2}}{U_{\infty 1}+U_{\infty 2}\sqrt{\rho_{\infty 2}/\rho_{\infty 1}}}\right] f(M_c) \tag{8}$$

with $f(M_c)$ given by Eq. (7). Note that the term inside the brackets accounts for the density effect on instability, which is to increase the growth rate if the fast stream is light and to reduce it if the fast stream is heavy.[5]

Model for the Wall Stresses

Accurate estimates for the wall stress τ_w of the compressible, turbulent boundary layer were obtained a long time ago by a large number of investigators. For adiabatic wall, we use Van Driest's[13] formula for the skin-friction coefficient c_f

$$0.242\sqrt{\frac{1-\lambda^2}{c_f}}\frac{\sin^{-1}\lambda}{\lambda} = \log(R_x c_f) + 1.26\log(1-\lambda^2)$$
$$1-\lambda^2 = \left(1+\frac{\gamma-1}{2}M_\infty^2\right)^{-1} \tag{9}$$

where R_x is the Reynolds number based on streamwise distance x and the relation $\mu \sim T^{0.76}$ has been assumed. The wall stress is then obtained by

$$\tau_W = c_f \tfrac{1}{2}\rho_\infty U_\infty^2 \tag{10}$$

Governing Equations

Having established approximate relations for the wall and dividing-streamline shear stresses, we now proceed to development of the governing equations. It is assumed that flow is fully developed turbulent and the layer thin enough for the usual boundary-layer approximations to hold. Furthermore, the turbulent Prandtl and Lewis numbers are taken to be unity ($Pr_t = 1$, $Le_t = 1$), which means that the exchange coefficients

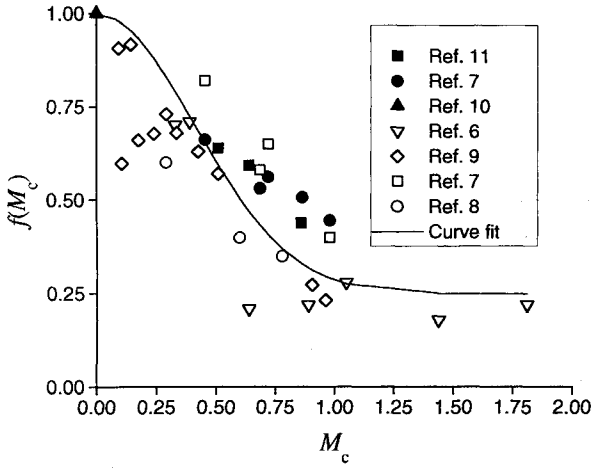

Fig. 2 Compressibility function $f(M_c)$ as inferred from LDV shear-stress managements (solid symbols) and growth-rate measurements (open symbols).

for momentum, heat, and mass are equal. Next are the equations for momentum, energy in terms of the total enthalpy $\bar{H}$, and species in terms of the mass fraction $\bar{C}_1$ of species 1

$$\bar{\rho}\frac{D\bar{u}}{Dt} = \frac{\partial}{\partial y}\left(\mu_t\frac{\partial\bar{u}}{\partial y}\right) = \frac{\partial\tau}{\partial y} \tag{11}$$

$$\bar{\rho}\frac{D\bar{H}}{Dt} = \frac{\partial}{\partial y}\left(\mu_t\frac{\partial\bar{H}}{\partial y}\right) = \frac{\partial q}{\partial y} \tag{12}$$

$$\bar{\rho}\frac{D\bar{C}_1}{Dt} = \frac{\partial}{\partial y}\left(\mu_t\frac{\partial\bar{C}_1}{\partial y}\right) = \frac{\partial\omega}{\partial y} \tag{13}$$

where

$$\frac{D}{Dt} \equiv \frac{1}{\bar{\rho}}\left(\overline{\rho u}\frac{\partial}{\partial x} + \overline{\rho v}\frac{\partial}{\partial y}\right)$$

Here, μ_t is the eddy viscosity, τ the turbulent (Reynolds) shear stress, q the heat transfer between the two streams, and ω the mass transfer between the two streams. The mass fraction $\bar{C}_1$ ranges between 0 (stream 2) and 1 (stream 1) and its counterpart $\bar{C}_2 = 1 - \bar{C}_1$. Note that the energy equation (12) is not restricted to single species and, therefore, can be applied to gas mixtures of variable composition.[14] Inspection of the preceding equations leads to the conclusion that both $\bar{H}$ and $\bar{C}_1$ must be linear functions of the velocity $\bar{u}$. For the energy equation, this leads to the well-known Crocco-Busemann relations (see, for example, Ref. 15). Expressed in terms of freestream conditions, these linear relations are

$$\bar{H} = \frac{U_{\infty 1}H_{\infty 2} - U_{\infty 2}H_{\infty 1}}{U_{\infty 1} - U_{\infty 2}} + \frac{H_{\infty 1} - H_{\infty 2}}{U_{\infty 1} - U_{\infty 2}}\bar{u} \tag{14}$$

$$\bar{C}_1 = -\frac{U_{\infty 2}}{U_{\infty 1} - U_{\infty 2}} + \frac{1}{U_{\infty 1} - U_{\infty 2}}\bar{u} \tag{15}$$

It is now easy to make the connection between q, ω, and τ by inserting the foregoing functions in their respective conservation equations and comparing with the momentum equation

$$q = \frac{H_{\infty 1} - H_{\infty 2}}{U_{\infty 1} - U_{\infty 2}}\tau \tag{16}$$

$$\omega = \frac{1}{U_{\infty 1} - U_{\infty 2}}\tau \tag{17}$$

Equations (16) and (17) illustrate how the shear stress "drives" the heat and mass transfer. They have been derived for zero pressure gradient. There is scant information in the

literature as to how they hold for finite pressure gradient. It will be assumed here that Eqs. (16) and (17) are still approximately valid under moderate pressure gradients. This is not a crucial assumption as the entropy generation turns out to be insensitive to pressure gradient, and the displacement-thickness analysis is carried out under conditions of near-zero pressure gradient.

We now consider the quasi-one-dimensional model of a shear layer with same stresses, heat transfer, and mass transfer as the two-dimensional model. The concept of mass transfer across the dividing streamline may seem contradictory at first. We must keep in mind that the dividing streamline is a *time-averaged* concept, whereas lumps of fluid can instantaneously traverse from one side of the layer to the other. Quantities are now uniform across each stream [$\bar{u}(x, y) \rightarrow U(x)$, $\overline{H}(x, y) \rightarrow H(x)$, etc.]. The quasi-one-dimensional conservation equations are obtained by setting $\overline{\rho v} = 0$ in the two-dimensional equations and integrating them over the height Y of each stream. In case of dissimilar gases, the composition of each stream will change with x as a result of the mass transfer (entrainment). The perfect gas relations $h(x) = c_p(x)T(x)$ and $p(x) = R(x)\rho(x)T(x)$ will be used. For each stream, we have the following set of equations

Mass:

$$\frac{d\rho}{\rho} + \frac{dU}{U} + \frac{dY}{Y} = 0 \tag{18}$$

Momentum:

$$U\,dU + \frac{dp}{\rho} = \frac{\tau\,dx}{\rho Y} \tag{19}$$

Energy:

$$dH = \frac{q}{\rho UY}dx \tag{20}$$

State:

$$\frac{dp}{p} = \frac{dR}{R} + \frac{d\rho}{\rho} + \frac{dT}{T} \tag{21}$$

Perfect gas:

$$\frac{dh}{h} = \frac{dc_p}{c_p} + \frac{dT}{T} \tag{22}$$

Species:

$$dC_1 = \frac{\omega}{\rho UY}dx = \frac{\tau\,dx}{\rho UY(U_{\infty 1} - U_{\infty 2})} \tag{23}$$

with Eq. (17) having been applied in the last relation. Equations (18–22) are now combined to give a differential expression for velocity in terms of Mach number

$$\frac{dU}{U} = \left[1 + \frac{\gamma - 1}{2}M^2\right]^{-1}\left[\frac{dM}{M} + \frac{1}{2}\left(\frac{q\,dx}{\rho UYh} + \frac{dR}{R} - \frac{dc_v}{c_v}\right)\right] \tag{24}$$

which leads to a differential equation for the Mach number itself

$$\frac{dM}{M} = \frac{1 + [(\gamma - 1)/2]M^2}{M^2 - 1}\left(\frac{\tau\,dx}{pY} + \frac{dc_p}{c_p} + \frac{dY}{Y}\right) - \frac{M(1 + \gamma M^2)}{2(M^2 - 1)}\left(\frac{q\,dx}{\rho UYh} + \frac{dR}{R}\right) + \frac{dc_v}{2c_v} \tag{25}$$

with the heat transfer q given by Eq. (16).

Equations (18–25) can be specialized to a particular stream by placing the appropriate subscript (1 or 2) under each variable. For the general case of viscous walls, the stresses τ_1 acting on stream 1 and τ_2 acting on stream 2 are

$$\tau_1 = -\tau_{\text{dsl}} - \tau_{W1}$$
$$\tau_2 = \tau_{\text{dsl}} - \tau_{W2} \tag{26}$$

The area variations are given by

$$\frac{dY_1}{dx} = -\frac{dy_{\text{dsl}}}{dx} + \frac{1}{2}\alpha$$
$$\frac{dY_2}{dx} = -\frac{dy_{\text{dsl}}}{dx} + \frac{1}{2}\alpha \tag{27}$$

Since this is a quasi-one-dimensional calculation, it is actually immaterial how the divergence angle α is distributed among the two channel walls. Here it is divided equally for the sake of symmetry only.

The variation in gas properties c_v, c_p, and $R = c_p - c_v$ is proportional to the change in mass fraction given by Eq. (23). Letting $G = (c_v, c_p, R)$, we have

$$\frac{dG_1}{dx} = (G_{\infty 1} - G_{\infty 2})\frac{dC_1}{dx} = \frac{G_{\infty 1} - G_{\infty 2}}{\rho_1 U_1 Y_1}\frac{\tau_{\text{dsl}}}{U_{\infty 1} - U_{\infty 2}}$$
$$\frac{dG_2}{dx} = (G_{\infty 1} - G_{\infty 2})\frac{dC_2}{dx} = \frac{G_{\infty 2} - G_{\infty 1}}{\rho_2 U_2 Y_2}\frac{\tau_{\text{dsl}}}{U_{\infty 1} - U_{\infty 2}} \tag{28}$$

The specific-heat ratio γ is then obtained from its definition $\gamma = c_p/c_v$.

Solution Method

For prescribed initial conditions at $x = 0$, the quasi-one-dimensional solution of the flowfield depends only on the location of the dividing streamline $y_{\text{dsl}}(x)$. The shape of the dividing streamline is found by requiring pressure continuity across it, i.e., $p_1 = p_2$ at each x location. The specifics of this procedure are discussed next.

Starting at $x = 0$, we choose a slope dy_{dsl}/dx for the dividing streamline. Let us first concentrate on stream 1. Since the conditions at $x = 0$ are known, the stress τ_1 is computed from Eqs. (26), (8), and (10). The heat transfer q is computed from Eq. (16). Equations (25) and (24) are integrated numerically over a small increment dx, yielding M_1, U_1, and the speed of sound $a_1 = U_1/M_1$ at the new location $x = dx$. The new area Y_1 is calculated from Eq. (27), and the gas properties c_{p1}, c_{v1}, R_1 are computed from Eq. (28), from which $\gamma_1 = c_{p1}/c_{v1}$. The pressure at $x = dx$ is then obtained from the integral mass conservation equation:

$$p_1 = \dot{m}_1 a_1/\gamma_1 M_1 Y_1$$

The exact same procedure is then followed for stream 2, yielding a pressure p_2 at $x = dx$. If p_1 and p_2 are unequal, a new dy_{dsl}/dx is selected and the integration started anew until the error $|p_1 - p_2|/p_1$ is of order 10^{-12}. A Newton-Raphson iteration technique is used for fast convergence. Once the new pressure has been calculated, we refer to the two-dimensional model to obtain the freestream quantities ($U_{\infty 1}$, $U_{\infty 2}$, etc.) from the well-known isentropic relations. The new stresses τ_1 and τ_2 and heat transfer q are then computed. Integration is advanced to the next x location and the entire iteration procedure is repeated. A FORTRAN program was written to perform the computation on a 486-33 MHz, IBM-compatible personal computer. Each flow case took about 10 s to compute.

Entropy Production

The entropy change in each stream is described by the basic thermodynamic relationship

$$ds = \frac{1}{T}\left[dh - \frac{dp}{\rho}\right]$$

Using the momentum equation (19) and the energy equation (20), the relation just given becomes

$$ds = \frac{1}{T}\left[\frac{q\,dx}{\rho U Y} - \frac{\tau\,dx}{\rho Y}\right] \tag{29}$$

from which we obtain an expression for the entropy flux $\dot{S} = \dot{m}\Delta s = \rho U Y \Delta s$ in each stream

$$\frac{d\dot{S}}{dx} = \frac{1}{T}[q - U\tau] \tag{30}$$

Expressing q in terms of τ according to Eq. (16), Eq. (30) becomes

$$\frac{d\dot{S}}{dx} = \frac{\tau}{T}\left[\frac{H_{\infty 1} - H_{\infty 2}}{U_{\infty 1} - U_{\infty 2}} - U\right] \tag{31}$$

Since we are only interested in entropy generation due to shear-layer mixing, and not in that due to wall friction, we consider inviscid walls and set $\tau_1 = -\tau_{dsl}$, $\tau_2 = \tau_{dsl}$. The expression for the combined entropy flux $\dot{S}_{12} = \dot{S}_1 + \dot{S}_2$ is

$$\frac{d\dot{S}_{12}}{dx} = \tau_{dsl}\left[\frac{U_1}{T_1} - \frac{U_2}{T_2} + \frac{H_{\infty 1} - H_{\infty 2}}{U_{\infty 1} - U_{\infty 2}}\left(\frac{1}{T_2} - \frac{1}{T_1}\right)\right] \tag{32}$$

We now examine two cases for Eq. (32), both in the near field where the values of the quasi-one-dimensional variables are close to the freestream values ($U_1 \approx U_{\infty 1}$, etc.). In the isothermal case, where $T_1 = T_2 = T$, Eq. (32) reduces to

$$\frac{d\dot{S}_{12}}{dx} \approx \frac{\tau_{dsl}}{T}\Delta U \tag{33}$$

Keeping in mind that $\tau_{dsl} \sim (\Delta U)^2$, we see that entropy is generated in the fashion $d\dot{S}_{12}/dx \sim (\Delta U)^3$.

For $c_{p1} = c_{p2} = c_p$, Eq. (32) can be rewritten as

$$\frac{d\dot{S}_{12}}{dx} \approx \frac{\tau_{dsl}}{T_{\infty 1} T_{\infty 2}}\left[T_{avg}\Delta U + c_p\frac{(\Delta T)^2}{\Delta U}\right] \tag{34}$$

To put the entropy rise in more practical terms, we define an equivalent total pressure ratio ψ, which is the ratio of the total pressure at $x = 0$ (unmixed conditions) to the total pressure at a downstream location x in a single adiabatic stream, with mass flux $\dot{m}_{12} = \dot{m}_1 + \dot{m}_2$ and entropy flux $\dot{S}_{12}$ as given by Eq. (32)

$$\psi \equiv \exp\left(-\frac{\dot{S}_{12}}{\dot{m}_{12} R_{12}}\right) \tag{35}$$

where

$$R_{12} = \frac{1}{\dot{m}_{12}}(\dot{m}_1 R_1 + \dot{m}_2 R_2)$$

is the equivalent gas constant for the combined two streams. Note that, as a result of species conservation, R_{12} is an invariant in the flowfield.

It is now instructive to see the relation between ψ and shear-layer compressibility measured in terms of the convective Mach number M_c. We will do this for the near field of the isothermal case with equal areas $Y_{01} = Y_{02} = Y_0$. From the definition of ψ in Eq. (35) we write

$$\frac{1}{\psi}\frac{d\psi}{dx} = -\frac{1}{\dot{m}_{12} R_{12}}\frac{d\dot{S}_{12}}{dx}$$

Substituting Eq. (33) for $d\dot{S}_{12}/dx$, and noting that $\dot{m}_{12} R_{12} = 2pY_0 U_{avg}/T$, we have

$$\frac{1}{\psi}\frac{d\psi}{dx} = -\frac{\tau_{dsl}}{2pY_0}\frac{\Delta U}{U_{avg}}$$

Relating the stress τ_{dsl} to the growth rate by virtue of Eq. (1) we obtain

$$\frac{1}{\psi}\frac{d\psi}{dx} = -\frac{0.077}{2Y_0}\frac{d\delta}{dx}\frac{(\Delta U)^2}{p/\rho_{avg}}$$

The constant 0.077 is the ratio of the constant 0.013 in the relation for shear stress [Eq. (8)] to the constant 0.17 in the relation for the growth rate [Eq. (5)]. The ratio p/ρ_{avg} can be manipulated into an expression involving the freestream speeds of sound so as to bring out M_c

$$\frac{1}{\psi}\frac{d\psi}{dx} = -\frac{0.019}{Y_0}\frac{d\delta}{dx}\left[\gamma_{\infty 1}\left(1 + \frac{a_{\infty 2}}{a_{\infty 1}}\right)^2 + \gamma_{\infty 2}\left(1 + \frac{a_{\infty 1}}{a_{\infty 2}}\right)^2\right]M_c^2 \tag{36}$$

It is actually more revealing to write Eq. (36) in the form

$$\frac{1}{\psi}\frac{d\psi}{d(\delta/Y_0)} = -0.019\left[\gamma_{\infty 1}\left(1 + \frac{a_{\infty 2}}{a_{\infty 1}}\right)^2 + \gamma_{\infty 2}\left(1 + \frac{a_{\infty 1}}{a_{\infty 2}}\right)^2\right]M_c^2 \tag{37}$$

which gives the rate of change of ψ with respect to the fraction of the channel area that the mixing region occupies. As an example, if we mix hydrogen and air at the same temperature ($\alpha_{\infty 1}/\alpha_{\infty 2} = 3.8$), Eq. (37) gives

$$\frac{1}{\psi}\frac{d\psi}{d(\delta/Y_0)} = -0.66M_c^2$$

For $M_c = 1.3$, we can quickly estimate that, at the point where $\delta = Y_0$, the loss in equivalent total pressure will be about 70%. This is in agreement with the more refined estimates obtained in the next section.

For unequal temperatures, the relation of ψ to M_c becomes too cumbersome to write here. Nevertheless, it is evident by examining Eqs. (32) and (34) that some form of Mach number based on velocity difference will factor strongly in those equations, hence the intrinsic compressibility of the flow will dominate entropy production and loss in total pressure.

Results

We will now employ the quasi-one-dimensional shear-layer model to situations that might arise in practical devices like supersonic-combustion engines or in laboratory experiments. The main quantities of interest are the entropy rise due to the shear layer, expressed in terms of the equivalent total pressure ratio ψ, and the streamwise pressure variation. The value of the channel divergence angle α for which the pressure variation between two selected stations in the flow is zero, is denoted α_{zpg}. For the case of inviscid walls, α_{zpg} is equal to the growth rate of the displacement thickness of the shear layer, expressed in degrees. For viscous walls, α_{zpg} represents the displacement-thickness growth rate of the combined shear layer and boundary layers. The value of ψ was computed under the condition $\alpha = \alpha_{zpg}$ in order to maximize the validity of Eqs. (16) and (17). Computations not presented here showed that even a strong pressure gradient affects ψ very little. In case 5 for example (see Table 1), ψ changed from 0.33 with $\alpha = \alpha_{zpg}$ to 0.37 with $\alpha = 0$, an 11% increase in the presence of a pressure rise of 400% over a streamwise distance of six channel heights.

Inviscid Walls

By considering the walls to be inviscid, we isolate the effect of the shear layer on pressure variation. The static pressure p and equivalent total pressure ratio ψ are evaluated at the point where the shear-layer thickness is half of the initial channel height, i.e.,

$$\delta = \tfrac{1}{2}(Y_{01} + Y_{02})$$

with δ obtained by Eq. (5).

Table 1 lists five cases to which the model with inviscid walls was applied. All five cases have $Y_{01} = Y_{02} = 1$. In case 1, the velocity difference is small, so the entropy rise is also small [see Eq. (32)] and the pressure variation with parallel walls ($\alpha = 0$) is slightly negative. The rest of the cases involve large velocity difference, and consequently high M_c. Cases 2 and 3 have same Mach numbers, density ratio, and velocity ratio. In case 2, the density and velocity ratios are achieved by mixing two air streams with different total temperatures, while in case 3 they are achieved by mixing air and hydrogen at the same total temperature. The pressure rise with $\alpha = 0$ and the value of α_{zpg} are identical in the two cases. However, ψ is substantially lower in case 2. Actually, the entropy flux $\dot{S}_{12}$ is similar in the two cases, but ψ for case 2 is lower because of the smaller $\dot{m}_{12}R_{12}$ [see Eq. (35)]. Cases 2–6 exhibit a pressure rise when $\alpha = 0$ and have positive α_{zpg}. Figure 3 shows the geometry of the dividing streamline and the variations of static pressure and ψ for case 3.

Cases 3–6 represent flow regimes with large velocity difference that might occur inside a supersonic combustor. It is seen that total pressure losses range from 30 to 70%. They are similar to losses associated with a normal shock in a single stream with Mach number ranging from 2 to 3! In a normal shock, the drop in total pressure is accompanied by a large increase in pressure and a decrease in Mach number to subsonic values. Here, under zero pressure gradient, the total pressure drop is connected to a decrease in Mach numbers from high- to low-supersonic values. Figure 4 shows the decline of M_1 and M_2 for case 3 at constant pressure.

Viscous Walls: Comparison with Experiments

There are no experiments known to the author designed specifically for measuring entropy rise (or total pressure loss) in shear layers. However, one may calculate the total pressure loss from pitot surveys that were used to infer the growth rate of shear layers. The total pressure loss manifests itself clearly when the freestream total pressures are close to each other, i.e., when the Mach numbers of the two streams are similar. Then, the pitot pressure distribution inside the shear layer shows a defect whose magnitude depends on the entropy rise.

Table 2 shows two such cases (6 and 7) from the experiments of Papamoschou and Roshko.[6] The author has in his possession the raw data for pitot and static pressures collected in the experiments. This enabled the calculation of the experimental equivalent total pressure ratio ψ for cases 6 and 7. In both cases, the initial areas were $Y_{01} = Y_{02} = 11$ mm. First, the total pressure was extracted from the pitot pressure using the Rayleigh pitot formula and assuming a hyperbolic-tangent variation of $\gamma(y)$ across the layer. The velocity and density distributions $u(y)$ and $\rho(y)$ were calculated assuming a similar distribution for the gas constant $R(y)$.

The resulting total pressure distributions $p_T(y)$ are shown in Fig. 5. Notice how prominent the defect is in case 7 (large ΔU) compared to case 6 (small ΔU). For both cases, $\Delta T \approx 0$, thus entropy is expected to rise at a rate roughly proportional to $(\Delta U)^3$ [see Eq. (33)]. Also shown in Fig. 3 are the presumed "isentropic" distributions $p_{Ti}(y)$ which represent the profiles one would expect if no losses occurred. They are obtained by fitting a hyperbolic-tangent profile between the freestream values. The entropy flux was calculated from the relation:

$$\dot{S}_{12} = -\int_{-Y_1}^{Y_2} \rho(y)u(y)R(y)\ell n(p_T/p_{Ti})\,dy$$

and ψ was obtained from Eq. (35).

Table 2 shows that the experimental and theoretical values of ψ compare rather well. In case 6, the quasi-one-dimensional model slightly overpredicts the value of ψ. Since this case has a small velocity difference ($U_{02}/U_{01} = 0.75$), the wake effect persists for long distance downstream and may enhance the defect in pitot-pressure profile, thus making ψ appear lower. In contrast, case 7 has a high velocity difference ($U_{02}/U_{01} =$

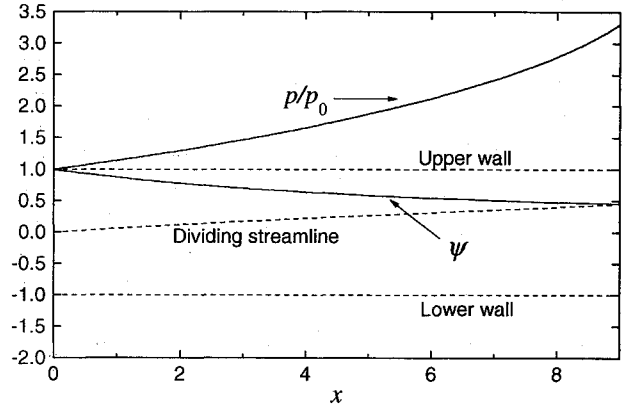

Fig. 3 Mixing geometry and variation in pressure and equivalent total pressure ratio ψ for case 3.

Table 1 Inviscid walls, pressures evaluated at $\delta = \frac{1}{2}(Y_{01} + Y_{02})$

Case	Gas 1	M_{01}	T_{T01}, K	Gas 2	M_{02}	T_{T02}, K	M_c	U_{02}/U_{01}	ρ_{02}/ρ_{01}	$\left(\frac{p}{p_0}\right)_{\alpha=0}$	ψ_{zpg}	α_{zpg}
1	Air	4	300	Air	2	300	0.37	0.76	0.4	0.98	0.89	−0.1
2	Air	2	4200	Air	3	300	1.12	0.32	22	3.57	0.04	6.8
3	H_2	2	300	Air	3	300	1.12	0.32	22	3.57	0.37	6.8
4	H_2	3	600	Air	3	1200	1.35	0.38	7	1.68	0.73	2.0
5	H_2	3	1200	Air	3	1200	1.73	0.26	14	4.01	0.33	8.1

Table 2 Viscous walls, comparison with experiments: $T_{T01} = T_{T02} = 300$ K

								ψ_{zpg}		α_{zpg}		
Case	Gas 1	M_{01}	Gas 2	M_{02}	M_c	p_0, atm	x/Y_{01}	Q1D[a]	Exp[b]	Q1D[a]	Exp[b]	Ref.
6	N_2	2.8	Ar	2.6	0.40	0.2	13	0.97	0.94	0.8	1.0	6
7	He	2.6	N_2	2.8	1.05	0.2	11	0.84	0.82	2.4	2.0	6
8	Ar	1.50	He	0.23	0.11	1.0	12	0.79	—	−1.8	−2.0	9
9	N_2	1.48	He	0.23	0.18	1.0	12	0.87	—	−2.3	−2.0	9
10	N_2	1.46	N_2	0.29	0.51	1.0	12	0.92	—	−2.6	−2.0	9
11	He	1.48	N_2	0.30	0.90	1.0	12	0.81	—	−1.8	−1.0	9
12	He	1.50	Ar	0.35	0.96	1.0	12	0.79	—	0.0	0.0	9
13	N_2	0.063	N_2	0.025	0.00	1.0	10	1.00	—	−1.0	−1.0	16

[a]Q1D = quasi-one-dimensional model. [b]Exp = experiment.

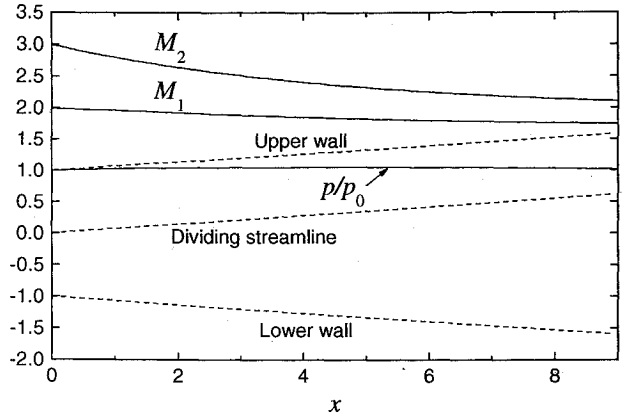

Fig. 4 Mixing geometry and variation in Mach numbers for case 3 under constant pressure.

0.4), consequently the wake effect is expected to vanish rapidly. Also shown in Table 2 are the experimental and theoretical values of α_{zpg}, which are in good agreement. Note that here α_{zpg} reflects the displacement thickness of the shear layer plus boundary layers.

The next set of comparisons (cases 8–12) are performed between the quasi-one-dimensional model and the shear-layer experiments of Hall,[9] in which the value of α_{zpg} was well documented for a large number of test cases. In Hall's experiments, the initial areas were $Y_{01} = 32$ mm and $Y_{02} = 51$ mm. On the average, the quasi-one-dimensional model predicts well the trends and the actual values of α_{zpg}. Figure 6 shows the axial pressure variation (in kPa) in case 10 with $\alpha = \alpha_{zpg}$. It is seen that pressure increases a few kPa (the absolute pressure is around 100 kPa) and then drops back to the initial value. Interestingly, Hall also observed the same trend in this and others of his cases.

Finally, case 13 is an incompressible shear layer from the experiments of Hermanson and Dimotakis.[16] The initial areas were $Y_{01} = 50$ mm and $Y_{02} = 75$ mm. The agreement between the quasi-one-dimensional and experimental value of α_{zpg} is very good. This shows that the quasi-one-dimensional model can also be applied to incompressible shear layers for predicting pressure variation.

In all of the viscous wall cases examined here, the pressure gradient with parallel walls ($\alpha = 0$) is adverse. The contribution of the combined boundary layers to the value of α_{zpg} listed in Table 2 ranges between 0.3 and 0.5 deg.

Discussion

The quasi-one-dimensional model has shown that substantial total pressure losses are likely to occur in compressible mixing with large velocity difference. Since most practical applications involve mixing between air and hydrogen (as in scramjet engines), it is inevitable that large ΔU will occur over the operating range of the device. In fact, high ΔU leads to faster mixing, which is desired for combustion. On the other hand, rapid mixing at compressible speeds is accompanied by high entropy production. Clearly, there are tradeoffs that depend on the characteristics of the specific application.

In actual devices, total pressure losses will undoubtedly be worse than predicted by this model. First, the dividing streamline is never straight, even if one starts with perfectly matched pressures (see Fig. 3). The bending of the dividing streamline generates compression and expansion waves, the former of which will eventually coalesce into oblique shocks. Second, the adverse pressure gradient in compressible cases with high ΔU may cause separation of the boundary layers. Unless the pressure gradient is canceled or minimized by appropriate geometry of the walls, separation will cause even higher losses and may lead to choking.

It is interesting to speculate on the microscopic mechanisms responsible for the large entropy production at high compressibility. A highly dissipative phenomenon is the formation of shock waves attached on the turbulent eddies, the so-called shocklets. Although experimental evidence of shocklets remains weak, computations of three-dimensional homogeneous turbulence do reveal their presence at high enough compressibility levels.[17] One unexpected feature seen in experimental investigations[18,19] of shear layers with M_c exceeding about 0.6 is that the convective velocity U_c approaches very closely one of the freestream velocities, rather than the average velocity U_{avg}. This happens even when the two densities are not very different. The "asymmetric" propagation of the turbulence structure has the potential of generating shocklets at smaller values of M_c than one might expect if $U_c \approx U_{avg}$. Also, at given M_c, the shocklets will be stronger if the eddies propagate asymetrically.

It appears thus possible that the flow somehow arranges for the eddy convective velocity to be such that the shocklets generate the amount of entropy dictated by the mean-flow

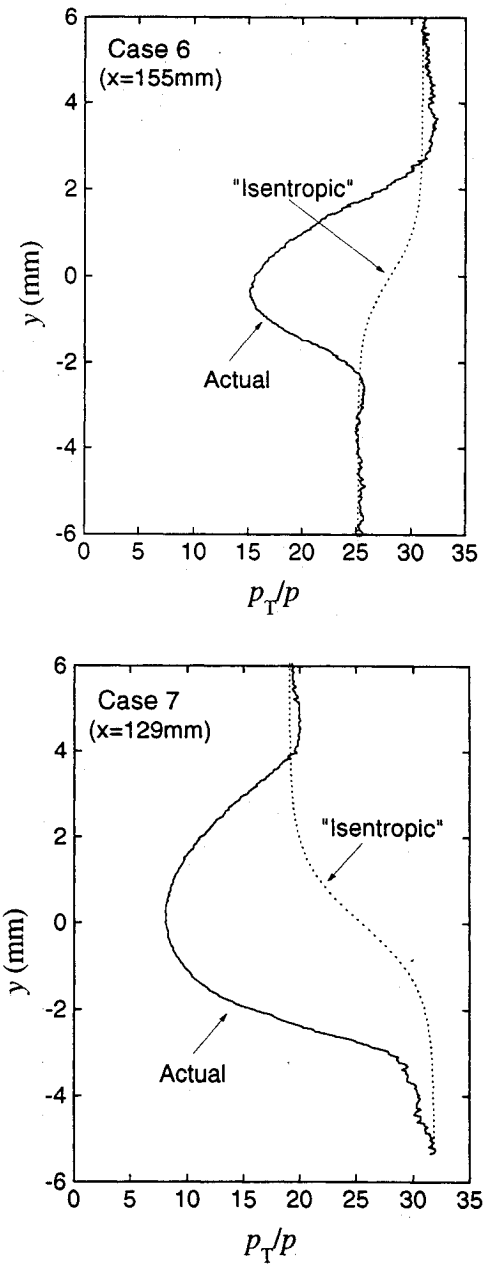

Fig. 5 Total pressure distributions for cases 6 and 7; inferred from experimental data of Ref. 6.

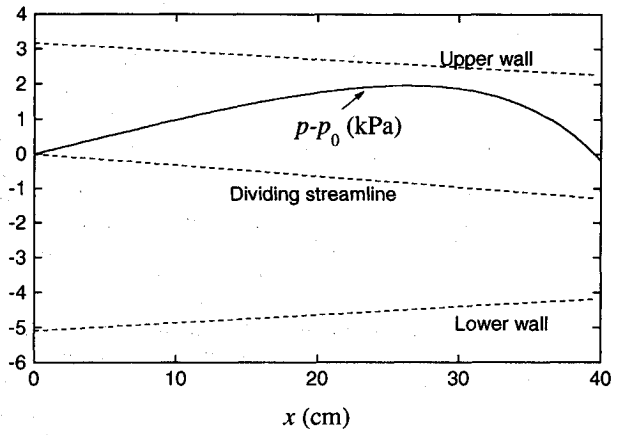

Fig. 6 Mixing geometry and pressure variation for case 10 vertical dimensions are in centimeters.

gradients and by the growth rate. On the other hand, the growth rate itself may be coupled to the behavior of the turbulent eddies. The possibility of such complex synergisms should serve as motivation for further analytical and experimental work on this subject.

Conclusions

A quasi-one-dimensional model for the planar, confined shear layer has revealed the potential for large entropy production and total pressure loss as the convective Mach number becomes of order one or higher. Even before the two streams are fully mixed, the losses due to mixing can be comparable to normal shock losses in a uniform stream of equivalent Mach number. The model compares well with the limited amount of available experimental data on total pressure loss.

With parallel channel walls, the usually adverse pressure gradient can be very strong, especially at high compressibility levels. The pressure gradient can be canceled by appropriate convergence or divergence of the channel walls, depending on the test case. This leads to estimates for the displacement thickness of the shear layer which compare favorably to experimental values found in the literature.

Acknowledgment

Discussions with S. E. Elghobashi have been very insightful.

References

[1]Ferri, A., and Edelman, R., "Some Observations on Heterogeneous Mixing Inside Channels," New York University Rept. NYU-AA-67-109, Aug. 1967.

[2]Ferri, A., "A Critical Review of Heterogeneous Mixing Problems," *Astronautica Acta,* Vol. 13, Nos. 5 and 6, 1968, pp. 453–465.

[3]Dutton, J. C., Mikkelsen, C. D., and Addy, A. L., "A Theoretical and Experimental Investigation of the Constant-Area, Supersonic-Supersonic Ejector," *AIAA Journal,* Vol. 20, No. 10, 1982, pp. 1392–1400.

[4]John, J. E. A., *Gas Dynamics,* 1st ed., Allyn and Bacon, Boston, 1969, pp. 174–176.

[5]Brown G. L., and Roshko A., "On Density Effects and Large-Scale Structures in Turbulent Mixing Layers," *Journal of Fluid Mechanics,* Vol. 64, No. 4, 1974, pp. 775–816.

[6]Papamoschou, D., and Roshko, A., "The Compressible Turbulent Shear Layer: An Experimental Study," *Journal of Fluid Mechanics,* Vol. 197, Dec. 1988, pp. 453–477.

[7]Goebel, S. G., and Dutton, J. C., "Velocity Measurements of Compressible Turbulent Shear Layers," AIAA Paper 90-0709, Jan. 1990.

[8]Clemens, N. T., Mungal, M. G., Berger, T. E., and Vandsburger, U., "Visualizations of the Structure of the Turbulent Mixing Layer Under Compressible Conditions," AIAA Paper 90-0550, Jan. 1990.

[9]Hall, J. H., "An Experimental Investigation of Structure, Mixing and Combustion in Compressible Turbulent Shear Layers," Ph.D. Thesis, Graduate Aeronautical Labs., California Inst. of Technology, 1991.

[10]Wygnanski, I., and Fiedler, H. E., "The Two-Dimensional Mixing Region," *Journal of Fluid Mechanics,* Vol. 41, April 1970, pp. 327–361.

[11]Elliott, G. S., and Samimy, M., "Compressibility Effects in Free Shear Layers," *Physics of Fluids A,* Vol. 2, No. 7, 1990, pp. 1231–1240.

[12]Townsend, A. A., *The Structure of Turbulent Shear Flow,* 2nd ed., Cambridge Univ. Press, London, 1976, p. 227.

[13]Van Driest, E. R., "Turbulent Boundary Layer in Compressible Fluids," *Journal of the Aeronautical Sciences,* Vol. 18, March 1951, pp. 145–160.

[14]Hayes, W. D., and Probstein, R. F., *Hypersonic Flow Theory,* 1st ed., Academic, New York, 1959, p. 327.

[15]White, F. M., *Viscous Fluid Flow,* 1st ed., McGraw-Hill, New York, 1974, p. 627.

[16]Hermanson, J. C., and Dimotakis, P. E., "Effects of Heat Release in a Turbulent, Reacting Shear Layer," *Journal of Fluid Mechanics,* Vol. 199, Feb. 1989, pp. 333–375.

[17]Lee, S., Lele, S. K., and Moin, P., "Eddy Shocklets in Decaying Compressible Turbulence," *Physics of Fluids A,* Vol. 3, No. 4, 1991, pp. 657–664.

[18]Papamoschou, D., "Structure of the Compressible Turbulent Shear Layer," *AIAA Journal,* Vol. 29, No. 5, 1991, pp. 680–681.

[19]Fourguette, D. C., Mungal, M. G., and Dibble, R. W., "Time Evolution of the Shear Layer of a Supersonic Axisymmetric Jet," *AIAA Journal,* Vol. 29, No. 7, 1991, pp. 1123–1130.